A Novel Small Peptide H-KI20 Inhibits Retinal Neovascularization Through the JNK/ATF2 Signaling Pathway

Ruonan Wang,[1–6] Yi Xu,[2] Chen Niu,[7] Xihui Gao,[7] and Xun Xu[1–6]

[1]Department of Ophthalmology, Shanghai General Hospital, Shanghai Jiao Tong University School of Medicine, Shanghai, China
[2]Department of Preventative Ophthalmology, Shanghai Eye Disease Prevention and Treatment Center/Shanghai Eye Hospital, Shanghai, China
[3]National Clinical Research Center for Eye Diseases, Shanghai General Hospital, Shanghai, China
[4]Shanghai Key Laboratory of Ocular Fundus Diseases, Shanghai General Hospital, Shanghai Jiao Tong University, Shanghai, China
[5]Shanghai Engineering Center for Visual Science and Photomedicine, Shanghai General Hospital, Shanghai Jiao Tong University, Shanghai, China
[6]Shanghai Engineering Center for Precise Diagnosis and Treatment of Eye Diseases, Shanghai, China
[7]MOE/NHC/CAMS Key Laboratory of Medical Molecular Virology, School of Basic Medical Sciences, Shanghai Medical College, Fudan University, Shanghai, China

Correspondence: Yi Xu, Shanghai Eye Disease Prevention and Treatment Center, Shanghai Eye Hospital, No. 380 Kangding Road, Shanghai, 200040, China; xxyoph@sina.com.
Chen Niu, MOE/NHC/CAMS Key Laboratory of Medical Molecular Virology, School of Basic Medical Sciences, Shanghai Medical College, Fudan University, Shanghai, China, No. 130 Dongan Road, Shanghai, 200032, China; chniu@fudan.edu.cn.

Received: April 16, 2020
Accepted: December 17, 2020
Published: January 13, 2021

Citation: Wang R, Xu Y, Niu C, Gao X, Xu X. A novel small peptide H-KI20 inhibits retinal neovascularization through the JNK/ATF2 signaling pathway. *Invest Ophthalmol Vis Sci.* 2021;62(1):16. https://doi.org/10.1167/iovs.62.1.16

Purpose. Abundant evidence has shown benefits of antivascular endothelial growth factor (anti-VEGF) therapies in neovascular eye diseases. However, the high cost, side effects, and inconvenience of frequent injections demand alternative novel drug candidates. This study aimed to analyze antiangiogenic effects of peptide H-KI20 and illustrated signaling mechanisms.

Methods. Live cell culture and tracing, wound healing assay, and tube formation were performed in human retinal microvascular endothelial cells (HRECs). The chick embryo chorioallantoic membrane and mouse oxygen-induced ischemic retinopathy model were applied to examine the effects of H-KI20 in vivo. The intracellular signaling pathways were examined. Molecular docking and surface plasmon resonance assay were used to validate the direct interaction of H-KI20 and c-Jun N-terminal kinase 2 (JNK2).

Results. H-KI20 had high penetration ability in vitro and in vivo. It inhibited motility, migration, and tube formation of HRECs, without cytotoxicity, and inhibited angiogenesis in vivo. Furthermore, H-KI20 treatment reduced the phosphorylation level of activating transcription factor 2 (ATF2) stimulated by VEGF via downregulating p-JNK. H-KI20 bound to JNK2 directly with a dissociation constant value of 83.68 µM. The knockdown of ATF2 attenuated VEGF-induced tube formation and decreased the movement speed of HRECs.

Conclusions. H-KI20 inhibited angiogenesis both in vitro and in vivo. The ratios of p-ATF2/ATF2 and p-JNK/JNK stimulated by VEGF were decreased by H-KI20, and H-KI20 targeted JNK2 directly. In addition, the pivotal role of ATF2 in VEGF-induced retinal neovascularization was elucidated for the first time. Taken together, H-KI20 displays potential for pathological retinal angiogenesis as a sustained and low-toxic peptide.

Keywords: small peptides, H-KI20, retinal neovascularization, JNK/ATF-2 signaling pathway, vascular endothelial growth factor

The number of individuals with diabetes is expected to rise to 642 million by 2040, and diabetic retinopathy (DR) is a common microvascular complication of diabetes.[1] Along with this, neovascular eye diseases, including retinopathy of prematurity and neovascular age-related macular degeneration (nAMD), lead to vision impairment and even blindness, causing serious public health problems with significant socioeconomic impacts. Previous studies showed that pathologic angiogenesis plays an important role in these ocular diseases.[2–4] Angiogenesis is a multistep process that includes proliferation, migration of endothelial cells, and formation of well-connected tubular networks.[5] Normal physiological angiogenesis is mediated by balancing the angiogenic inhibitors and stimulators. However, an imbalance between these occurs during pathological angiogenesis with the overexpression of vascular endothelial growth factor (VEGF).[6]

Thus antiangiogenic treatment, especially the anti-VEGF therapy, is regarded as a major therapeutic strategy for these diseases, including aflibercept (Eylea;

Regeneron Pharmaceuticals, Tarrytown, NY, USA), ranibizumab (Lucentis; Genentech Inc., San Francisco, CA, USA), bevacizumab (Avastin; Genentech Inc.), and conbercept (Langmu; Kanghong, Inc., Sichuan, China).[7–9] However, the efficacy of VEGF inhibitors depends on the baseline of visual acuity. Two clinical trials reported that frequent injections increased the risk of geographic atrophy and was characterized by a gradual and irreversible loss of choriocapillaris, retinal pigment endothelium (RPE), and photoreceptors.[10,11] Also, repeated and frequent injections were associated with chronic ocular hypertension that lasted for several months or longer.[12] Because of these unmet medical needs, other alternative therapies are urgently needed. Recent advancements in ocular drugs led to the discovery of small peptides with low molecular weight, stable production methods, high solubility and penetration ability, less toxicity, reduced immunogenicity, and improved bioavailability through optimization, which displayed good potential for treating ocular neovascular diseases.[13,14] For example, angiostatin, which is a proteolytic fragment of plasminogen consisting of one to four kringles, has been reported to reduce retinal vascular permeability by downregulating the expression of VEGF in diabetic rat models.[15] The kringle domain, which usually consists of approximately 80 amino acids and contains three disulfide bonds, was originally discovered in the structure of prothrombin and then identified in a variety of proteins, including apolipoprotein (a), hepatocyte growth factor (HGF), and tissue plasminogen activator (tPA).[16,17] In this study, a novel 20–amino acid peptide, H-KI20, was synthesized as an analog of kringle 1 from HGF, which was previously reported to have antiangiogenic effects.[18,19]

Mitogen-activated protein kinase (MAPK) signaling is one of the key downstream signaling pathways and regulatory cascades triggered by the activation of VEGFR2, including p38-MAPK, c-Jun N-terminal kinase (JNK). And activating transcription factor 2 (ATF2) is an important downstream transcription factor.[20–22] ATF2 is a member of ATF and cyclic adenosine monophosphate–response element–binding protein (CREB) family containing basic leucine zipper domain. It functions in various cellular behaviors in response to stress or cytokines through heterodimerization or homodimerization with other AP1 family members, including Jun, Fos, CREB, and Maf.[23] For example, ATF2 is known to be involved in the repair of DNA double-strand breaks induced by ionizing radiation or lesions induced by ultraviolet radiation.[24] Apart from regulating cellular processes, alterations in ATF2 showed an association with the pathologies of various diseases. For example, increased expression of nuclear ATF2 has been reported to manage oncogenesis in synovial sarcoma by assembling with fusion oncoprotein SS18-SSX.[25] Besides, ATF2 was related to high-fat diet-induced obesity via adipocyte differentiation.[26] Although it has been reported that ATF2 was associated with the death of retinal ganglion cells (RGCs) caused by axonal injury[27] and promoted the proliferation and migration of RPE cells in DR,[28] the role of ATF2 in retinal pathological neovascularization has not been completely elucidated.

Hence, in this study, both in vitro and in vivo experiments were conducted to investigate the effects of H-KI20. Moreover, H-KI20 was shown to interfere with the JNK/ATF-2 signaling pathway.

Material and Methods

Peptides and Reagents

Peptide H-KI20 (IIGKGRSYKGTVSITKSGIK), scramble control peptide H-KI20S (GTGISKSKRKKTISIVIYGG) and FITC-labeled H-KI20 were synthesized by China Peptides Co., Ltd. (SuZhou, China). HRECs were purchased from Cell System (Kirkland, WA, USA) and cultured in complete classic medium with 10% serum and CultureBoost (ThermoFisher Scientific, Waltham, MA USA). Recombinant human $VEGF_{165}$ was obtained from R&D System (MN, USA). Anti-mouse VEGF antibodies were purchased from Sigma–Aldrich (St. Louis, MO, USA). Bevacizumab (Avastin) was purchased from Genentech (San Francisco, CA, USA). Growth factor reduced Matrigel matrix was obtained from BD Bioscience (Franklin Lakes, NJ, USA). Antibodies against ATF-2(Cat no. 35031), phospho-ATF2 (Thr71) (Cat no. 24329), SAPK/JNK (Cat no. 9252), and phospho-SAPK/JNK (Cat no. 4668) were purchased from Cell Signaling Technology (Danvers, MA, USA). Antibodies against p38 (Cat no. ab170019) and phospho-p38 (Cat no. ab178867) were purchased from Abcam (Cambridge, MA, USA). Antibodies against TFAP4 were purchased from Proteintech (Cat no. 12017; Rosemont, IL, USA). Antibodies against NFAT5 (Cat no. 35480) and phospho-NFAT5 (Cat no. 12146) were purchased from SAB (Baltimore, MD, USA). Recombinant human protein JNK2 was purchased from ThermoFisher (PR6568B).

Stability Assay of H-KI20 in Aqueous Solutions

The stability of H-KI20 in various aqueous solutions was examined as described previously[29] with a slight modification. Briefly, the lyophilized H-KI20 by adding water or buffer reached a final concentration of 200 µg/mL. The buffers included were as follows: (1) PBS pH 7.4; (2) Hanks balanced salt solution pH 7.4; (3) balanced salt solution Plus (BSS Plus; Alcon, Geneva, Switzerland) sterile intraocular irrigating solution, which was used to imitate the intraocular condition during all intraocular surgical procedures; (4) citrate buffer pH 4; and (5) citrate buffer pH 6. The prepared solutions were immediately frozen, stored, and were used as controls. The other solutions were incubated at 4°C or 37°C for four, 48, or 72 hours and then stored at −80°C. All samples were thawed at room temperature before being tested using HPLC. The relative concentration was calculated as follows: sample peak area/control peak area × 100%.

Cellular Uptake of H-KI20

HRECs were plated on six-well plates (2×10^5 per well) in a complete medium. After reaching the required confluence, cells were transferred into the complete medium containing FITC-labeled H-KI20 (prepared as described in)[30] at a concentration of 200 µM. After incubation for 15 minutes, 12 hours, and 24 hours, cells were treated with "CellMask Orange plasma membrane stain" (ThermoFisher) for 10 minutes and then washed with PBS thrice to remove extracellular bound peptides and stains. Cells were immersed in 1 mL PBS in each well and photographed using an automated upright fluorescence microscope (IX53; Olympus, Tokyo, Japan) to assess the internalization of H-KI20.

Flow Cytometry Quantitative Analysis

Flow cytometry experiments were performed as described in a previous study.[31] Briefly, HRECs were seeded on a 30-mm plate (1×10^6 per well). After reaching the desired confluence, cells were incubated with a complete medium containing FITC-labeled H-KI20 at a concentration of 200 µM for 30 minutes, 1 hour, 6 hours, 12 hours, and 24 hours. After being washed and trypsinized, they were suspended in 300 µL of PBS, transferred into Eppendorf centrifuge tubes, and stored in the dark until analysis. The number of FITC-labeled cells and the mean fluorescence intensity were measured using a cytometer (Cytoflex; Beckman Coulter Life Sciences, Indianapolis, IN, USA). Results were analyzed using FlowJo software (Tree Star Inc, Ashland, OR, USA).

Cytotoxicity

HRECs were seeded into 96-well plates at a density of 1×10^6/well. They were treated with VEGF or H-KI20. The cytotoxicity of H-KI20 on HRECs was assessed using MTS (3-(4,5-dimethylthiazol-2-yl)-5-(3-carboxymethoxyphenyl)-2-(4-sulfophenyl)-2H-tetrazolium) (Promega, Madison, WI, USA) following the manufacturer's protocol.

Cell Migration Assay

A cell migration assay was performed as described in a previous study.[32] Briefly, HRECs were plated at a density of 5×10^5 cells on a 12-well plate. After reaching 90% confluence, they were starved in the serum for 24 h and then wounded by manually scraping with a sterile 200-µL pipette tip. Cells were then treated with a complete medium with or without 25 ng/mL VEGF, or additional 200 µM of H-KI20, H-KI20S, or 12.5 mg/mL bevacizumab. After incubation for 10 hours at 37°C in 5% atmosphere, cells were photographed under a light microscope. Three fields (left, middle, and right) along the scratch were selected from each well under magnification ×10, and the percent migration was quantified using NIH ImageJ 1.32 software.

Tube Formation Assay

The tube formation assay was performed as described previously.[33] Briefly, approximately 2×10^4 HRECs were seeded on a Matrigel precoated 96-well plate (89646; ibidi USA, Fitchburg, WI, USA). After incubation with or without 25 ng/mL VEGF at 37°C for four hours, the tube formation was photographed under a light microscope, and three fields were randomly selected from each well. The total tube length and the number of branch points were quantified using NIH ImageJ 1.32 software.

High-Content Image Analysis

The high-content image analysis was performed similarly to that described previously.[34] Briefly, approximately 3×10^4/well HRECs were plated on a 12-well plate and incubated overnight, which allowed cell attachment to the bottom of the plate. For ATF2-siRNA2 transfection, cells were additionally cultivated overnight. VEGF, Avastin, or H-KI20 compounds were added two hours before the analysis. All the groups were then incubated in an Operetta high-content analysis system (PerkinElmer, New York, NY, USA) and photographed for 48 hours. Images were analyzed using the Harmony software. Roundness is a common measurement for quantifying the cell shape. It is normalized to give 1.0 for a perfect circle, while decreases in elongated and irregular objects.

Histologic Examination

On the fifth day after the intravitreal injection of H-KI20, mice were euthanized, and the enucleated eyes were fixed with 4% paraformaldehyde for a minimum of 24 hours. Eyes were sectioned, stained with hematoxylin-eosin (HE), and assessed using light microscopy.

Laser Photocoagulation and H-KI20 Penetration Ability in Vivo

The mouse model of choroidal neovascularization was induced by laser photocoagulation similarly to that described previously.[35] Adult C57BL/6J mice were anesthetized, and their pupils were dilated with 1% atropine sulfate oculentum (Santen, Osaka, Japan) before modeling. Two minutes after pupil dilation, ofloxacin eye ointment (AdvaCare Pharma, Shanghai, China) was applied to the cornea as a hemispherical magnifying lens. Four laser burns were induced typically at 3, 6, 9, and 12 o'clock positions around the optic disc in each eye using a green Argon laser pulse with a wavelength of 532 nm, a duration of 100 ms, a fixed diameter of 50 µm, and a power level at 120 mW.

On day 7 after laser photocoagulation, mice were sacrificed one hour after topical instillation of 6 µL of FTIC-labeled H-KI20 (2 mM) six times at 10-minute intervals under direct vision. Eyes were enucleated, fixed with 4% paraformaldehyde overnight, and dehydrated in 30% sucrose solution for six hours. Then, they were embedded in Tissue-Tek O.C.T Compound (Sakura Finetek USA, Inc., Torrance, CA, USA), sectioned, and stained with Alexa Fluro 568 conjugated isolectin B4 (Abcam) and DAPI. The dyed sections were then observed under a confocal laser scanning microscope (LSM 510; Carl Zeiss Meditec, Zurich, Switzerland).

Quantification of H-KI20 in Ocular Tissues After Topical Instillation

On day 7 after laser photocoagulation, mice were treated as mentioned earlier ($n = 3$ per group). Concentrations of H-KI20 in the sclera–choroid–RPE complex and retina after 0.5, 1, and 3 hours' topical instillation were analyzed on a Q Exactive HFX Orbitrap (ThermoFisher Scientific) equipped with a nano-UPLC system (EASYnLC1200) similarly to that described previously.[36] Briefly, samples were digested with trypsin (Promega, Madison, WI, USA) and spiked with 100 ng/mL stable-isotope-labeled H-KI20 as an internal standard. For each sample, 1 µg of total digested peptides were separated and analyzed. The separation was performed using a reversed-phase column (100 µm ID × 15 cm; Reprosil-Pur120 C18AQ,1.9 µm; Dr. Maisch HPLC GmbH, Ammerbuch, Germany). The mobile phases were H_2O with 0.1% FA, 2% ACN (phase A) and 80% ACN, 0.1% FA (phase B). The separation of samples was executed with a 30-minute gradient at a flow rate of 300 nL/min. Gradient B: 25% for two minutes, 5% to 22% for 18 minutes, 22% to 45% for six minutes, 45% to 95% for two minutes, and 95% for two minutes. Parallel reaction monitoring (PRM) was performed in centroid and positive modes with an Orbitrap analyzer at

Investigative Ophthalmology & Visual Science

a resolution of 15,000 (@200 m/z) for MS2. The predefined inclusion ions were fragmented using HCD with a normalized collision energy of 27% and an isolation window of 0.7 m/z. Raw data were processed using skyline software, and the quantification analysis was performed with the freeQuant module.

Chick Embryo Chorioallantoic Membrane (CAM) Assay

The CAM assay was performed as previously described.[37] Briefly, three-day-old shell-less fertilized eggs were incubated until day 8. After that, 5 µL of 0.01 M PBS, 10 µg/µL H-KI20, and 10 µg/µL H-KI20S were applied. After another 72 hours of incubation, capillaries were imaged using an Olympus SZX16 stereoscope. A total of 11 eggs were evaluated in each group.

In Vivo Oxygen-Induced Retinopathy (OIR) Assay in Mice

To further evaluate the antiangiogenic efficacy of H-KI20 in vivo, an OIR assay in mice was performed as previously described[38] with few modifications. The pregnant female C57BL/6J mice were provided by Shanghai Laboratory Animal Center of the Chinese Academy of Science. The animal experiment protocol adhered to the National Institutes of Health guide for the care and use of laboratory animals (NIH Publications No. 8523, revised 1996) and the ARVO Statement for the Use of Animals in Ophthalmic and Vision Research. Neonatal mice were randomly divided into five groups ($n = 4$ per group): (1) room air as control; (2) oxygen + PBS; (3) oxygen + H-KI20; (4) oxygen + H-KI20S; and (5) oxygen + anti-mouse VEGF antibodies. Briefly, on postnatal day 7 (P7), neonatal mice were exposed to 75% ± 2% oxygen until P12. Intravitreous injections of peptides at a concentration of 50 mM and PBS were given on P12 and P14, whereas a VEGFab (50 ng/µL) injection was given on P12. The retina was fixed with 4% paraformaldehyde for one hour and dissected on P17. The retina was blocked for 2 h with 5% *w/v* of bovine serum albumin containing 1% Triton X-100. Next, samples were incubated with Alexa Fluro 568–conjugated isolectin B4 (1:500) in blocking solution overnight at 4°C. These samples were then divided into four equal-sized quadrants, and the fluorescein images were captured. Furthermore, the eyes were fixed with 4% paraformaldehyde for 24 hours and embedded in paraffin for sections ($n = 6$ per group). The serial sections (10 µm) were stained using HE.

Western Blot Analysis

HRECs were cultured as described earlier. After treatment for 24 hours, the whole-cell protein lysates were extracted using RIPA lysis buffer (Epizyme, Shanghai, China) containing 1× protease inhibitors and phosphatase inhibitors (Solarbio, Beijing, China). Then, 20 µg proteins from each sample were loaded onto SDS-PAGE gels and subsequently transferred onto a polyvinylidene fluoride (PVDF) membrane. The membrane was incubated with primary antibodies overnight at 4°C after blocking with 5% nonfat milk. Tubulin expression was used as an internal control.

Molecular Docking

The structure of H-KI20 was built using protein build module in Molecular Operating Environment (MOE) software.[39] The x-ray structure of proteins were downloaded from the RCSB Protein Data Bank. MOE-Dock was used for molecular docking. The position of the original ligand in the x-ray structure of each protein was defined as the binding site. The docking workflow followed the "induced fit" protocol in which the side chains of the receptor pocket were allowed to move according to ligand conformations, with a constraint on their positions. The weight used for tethering side-chain atoms to their original positions was 10. All docked poses were ranked by London dG scoring first, after which a force field refinement was carried out on the top 30 poses followed by a rescoring of GBVI/WSA dG. The conformation with the lowest free energy of binding was selected as the best (probable) binding mode.

Surface Plasmon Resonance Assay

Biacore T200 instruments (GE Healthcare) were used to evaluate the binding affinity of H-KI20 to JNK2 via surface plasmon resonance (SPR). Briefly, after conditioning with 500 mM EDTA and 100 mM NaOH, 27.5 µg/mL of JNK2 was captured on the surface of the NTA chip at a flow rate of 10 µL/min in PBS with 0.05% (v/v) Tween-20. Serial concentrations of peptides were injected into the flow system and analyzed. The binding analysis was performed in PBS with 0.05% (v/v) Tween-20, pH 7.4, at 25°C. The association time was set to 120 seconds, whereas the dissociation time was set to 180 seconds. Before analysis, double reference subtractions were made to eliminate bulk refractive index changes, injection noise, and data drift. The binding affinity was determined by global fitting to a Langmuir 1:1 binding model within the Biacore Evaluation software (GE Healthcare, Chicago, IL, USA).[40]

Transfection

Cells were seeded in 12-well plates (3×10^4 cells/well). After 24 hours, the cells were transfected with ATF2 siRNA (GenePharma, Shanghai, China) or its corresponding negative control using Lipo2000 (ThermoFisher) following the manufacturer's protocol. The sequences of three ATF2 siRNAs were as follows: siRNA1: 5′-CCUGUGGAAUAUGAGUGAUTTAUCACUCAUAUUCCACAGGTT-3′; siRNA2: 5′-CGAGUCCAUUUGAGAAUGATTUCAUUCUCAAAUGGACUCGTT-3′; siRNA3: 5′-CCUCUUGCAACACCUAUCATTUGAUAGGUGUUGCAAGAGGTT-3′.

Statistical Analysis

All values were presented as means ± standard error of the mean. Data processing was conducted using GraphPad Prism 6.0 (GraphPad Software Inc, San Diego, CA, USA) or SPSS 22.0 (IBM, Armonk, NY, USA). One-way analysis of variance was performed, and statistical significance was defined as $P < 0.05$ (*) and $P < 0.01$ (**).

Investigative Ophthalmology & Visual Science

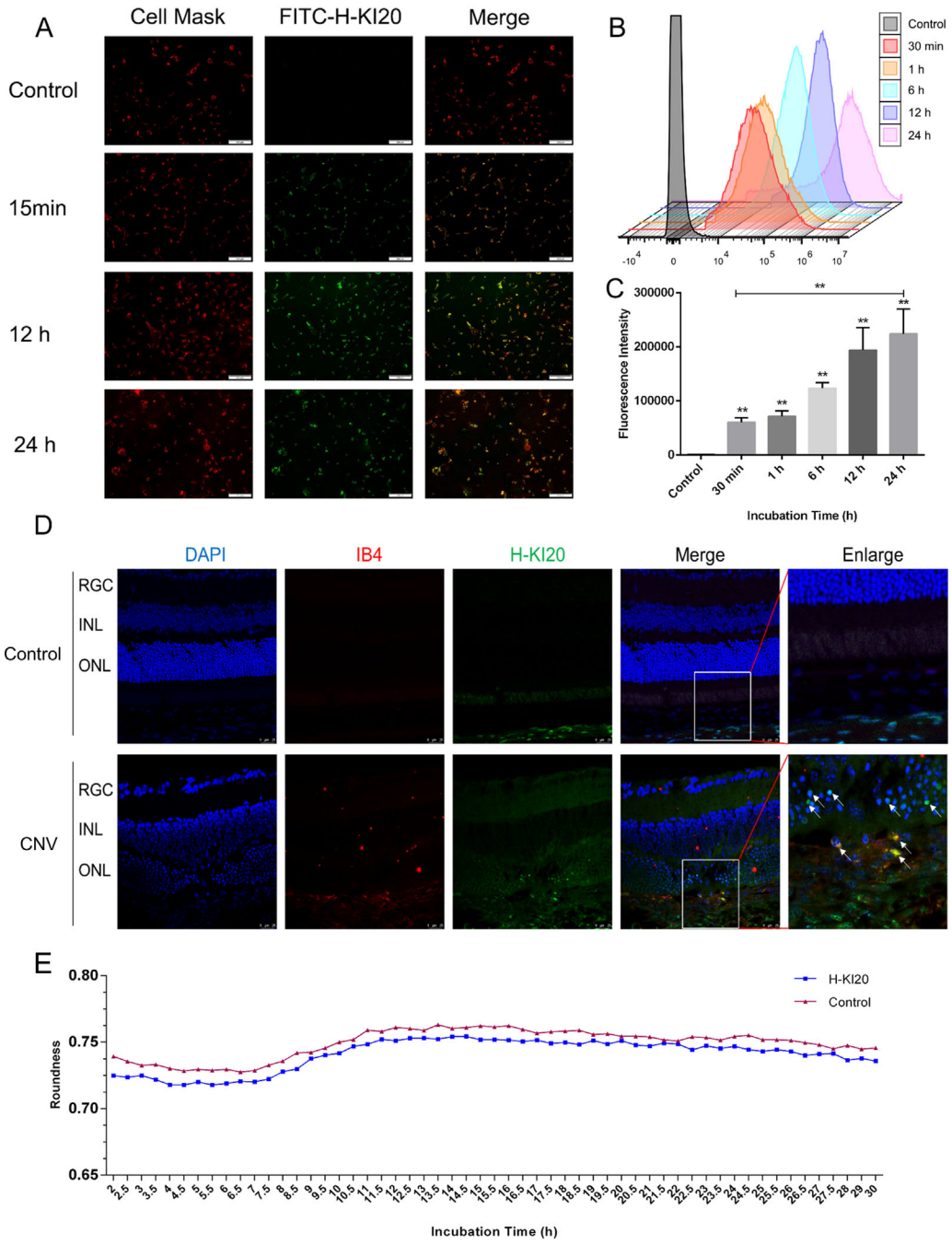

Figure 1. Peptide H-KI20 displayed high penetration ability and low toxicity in vitro and in vivo. (**A**) Fluorescent images of HRECs exposed to 200 µM FITC-labeled H-KI20 for 15 minutes, 12 hours, and 24 hours. *Scale bar*: 200 µm. CellMask, an orange plasma membrane stain; (**B** and **C**) flow cytometry quantitative analysis of H-KI20 revealed intake by HRECs. Fluorescence intensity was presented as means ±SEM, $^{*}P < 0.05$, $^{**}P < 0.01$, three independent assays were performed. (**D**) Fluorescent images of retina sections stained with IB4 and DAPI one hour after topical instillation of FITC-labeled H-KI20 at day 7 after laser photocoagulation. IB4: isolectin B4. *Scale bar*: 25 µm. $n = 3$ per group. (**E**) Cell roundness of HRECs incubated with or without H-KI20 was analyzed by Operetta high-content analysis (HCA) system (PerkinElmer) in a time series with an interval of 0.5h.

Results

H-KI20 Displayed a High Permeability in HRECs with High Stability and Low Cytotoxicity

H-KI20 was synthesized as an analogue of kringle I of HGF. An FITC-tagged H-KI20 was used to test the cellular permeability, and the fluorescence intensity in HRECs was measured. As shown in Figure 1A, the FITC-H-KI20 entered HRECs at 15 minutes after addition, and the fluorescence was increased in a time-dependent manner for 24 hours (the last test time point). Flow cytometry results revealed that the cells treated with H-KI20-FITC for 30 minutes displayed a mean fluorescence intensity (MFI) of 217-fold compared with untreated cells. Moreover, the MFI of cells after 24 hours increased to 3.67-fold compared

with that after 30 minutes, and this was consistent with fluorescence microscopy images (Figs. 1B and 1C). The results indicated that H-KI20 displayed good penetration ability in vitro. Moreover, the penetration ability of H-KI20 in vivo was evaluated in the laser-induced choroid neovascularization model. Seven days after laser photocoagulation, the retina sections were immunostained with IB4 and DAPI after the topical instillation of FTIC-labeled H-KI20. As shown in Figure 1D, the retina sections of control group only exhibited a distinct green band in the RPE–choroid–sclera complex, whereas in the choroidal neovascularization (CNV) group, fluorescence was detected within the retina or colocalized with isolectin B4, illustrating the appearance of neovessels and microglia cells in the CNV region. In addition, the PRM assay was used to quantify the concentrations of H-KI20 in the RPE–choroid–sclera complex and retina after topical instillation. As shown in Supplementary Figure S1, the mean concentration of H-KI20 at 0.5 hour after topical instillation was 33.8 ng/mL in the RPE–choroid–sclera complex, which was higher than that in the retina (20.5 ng/mL), and it was maintained for at least three hours.

In addition, the stability of H-KI20 was analyzed in different solutions (Supplementary Figs. S2A and S2B). Compared with the H-KI20 at 37°C, the H-KI20 at 4°C was more stable (Supplementary Fig. S2A). Although peptides were partially degraded after incubation for 24 or 48 hours in H_2O and PBS, the peptides had high stability in the remaining four buffers, with concentrations higher than 95% after 48 hours (Supplementary Fig. S2B). In addition, the application of H-KI20 at different concentrations showed no effect on the proliferation of HRECs (Supplementary Fig. S2C), indicating that H-KI20 did not cause any cytotoxicity. Furthermore, the cell morphology on H-KI20 treatment was examined through high-content analysis (Fig. 1E). Compared with the control group, H-KI20 treatment for 30 hours alone demonstrated no effect on the roundness of cells. Further, 50 or 75 mM H-KI20 was administered via intravitreal injection to examine the toxicity in vivo. All layers of the retina were normal and intact, without edema or inflammatory or immune reactions five days later (Supplementary Fig. S2D).

H-KI20 Inhibited VEGF-Induced Endothelial Cell Migration and Tube Formation

Next, the anti-angiogenic effects of H-KI20 were examined on HRECs. First, HRECs with 25 ng/mL VEGF stimulation displayed a 1.3-fold wound closure ($P < 0.05$) after 12 hours compared to the control group without VEGF or H-KI20 (Figs. 2A and 2B), indicating that VEGF functionally induced the migration of HRECs. Meanwhile, the treatment with Avastin, a commercially available anti-VEGF drug, inhibited the migration of cells significantly.[41] H-KI20 did not alter the migration of HRECs in the absence of VEGF, whereas it reversed the migration of VEGF-stimulated cells back to the level of the control group. The scrambled peptide H-KI20S showed no significant effect on the migration of HRECs. In addition, the movement speed was evaluated by high-content analysis (HCA) (Fig. 2C). The results revealed that H-KI20 abrogated the increase in the movement speed of HRECs stimulated by VEGF, whereas Avastin (2.5 mg/mL) showed no effect. The current speed was continuously monitored from two to 30 hours using HCA at an interval of 0.5 hour. At the initial time point, the current speed of cells in the control group was 0.006019 µm/s, and this was boosted by VEGF to 0.006486 µm/s but inhibited by H-KI20 to 0.006191 µm/s. This difference continuously existed for 30 hours until the end of the experiment, and the maximum difference among these groups was shown at 20 hours.

Second, the tube and loop formations of HRECs were quantified by measuring the tube length and branch points (Figs. 2D, 2E, and 2F). Compared to the control group, 25 ng/mL VEGF promoted the formation of tube-like structures on Matrigel, which was significantly inhibited by Avastin. H-KI20 also effectively inhibited VEGF-induced tube formation. No significant difference was found between VEGF and VEGF + the scrambled peptide H-KI20S.

H-KI20 Suppressed Angiogenesis Through JNK/ATF2 Signaling

VEGF mediated multiple cellular pathways through various transcriptional factors. The total and phosphorylated protein expression of ATF2 (Fig. 3A), nuclear factor of activated T-cells 5 (NFAT5), and transcription factor AP-4 (TFAP4) was analyzed (Supplementary Figs. S3A and S3B). Among these, the phosphorylated protein expression of ATF2 only increased, whereas the expression of NFAT5 and TFAP4 remained unchanged. The phosphorylated ATF2 expression was upregulated to 1.5-fold in VEGF-treated HRECs compared to the control group, which was abrogated by H-KI20 addition, whereas H-KI20 itself had no effect on phosphorylated ATF2 expression in the absence of VEGF (Fig. 3A). The phosphorylation of ATF2 was regulated by MAPKs, and therefore the expression of p38, JNK, and their phosphorylated form was tested.[20–22] Results showed that the phosphorylated JNK expression was twofold in the VEGF-stimulated group, which acted as the control and was restored by H-KI20 to the expression in the control group (Fig. 3B). In contrast, the phosphorylation of p38 (Supplementary Fig. S3C) was unaffected by H-KI20.

The ATF2 expression in HRECs was successfully disrupted by siRNA2 to validate ATF2 signaling in VEGF-induced angiogenesis (Fig. 4A). As shown in Figure 4E, the knockdown of ATF2 did not affect cell roundness, which was consistent with the effect on cells treated with H-KI20 (Fig. 1E). Also, the knockdown of ATF2 remarkably attenuated tube formation in HRECs (Figs. 4B, 4C, and 4D). In addition, the current speed that indicated cell movement decreased 31 hours after siRNA transfection (the initial time point). The current speed in the control group was 0.004876 µm/s and was boosted by VEGF to 0.005523 µm/s, but it was inhibited by siATF2 to 0.004701 µm/s. The difference continuously existed for 48.5 hours until the end of the experiment (Fig. 4F).

Interaction of H-KI20 with JNK2 Validated by Molecular Docking and SPR

To further investigate interactions between H-KI20 and JNK, and/or other upstream proteins regulating ATF2, docking score of 29 proteins with H-KI20 were calculated in MOE software (Table). A more negative score representing the binding energy indicated a better binding of the peptide with the protein. The interaction of H-KI20 with JNK2 was further explored because it had the maximum negative score. The calculations revealed the presence of seven hydrogen bonds between H-KI20 and JNK2 (Figs. 5A and 5B). As illustrated earlier, the docking simulation studies indicated that the

Investigative Ophthalmology & Visual Science

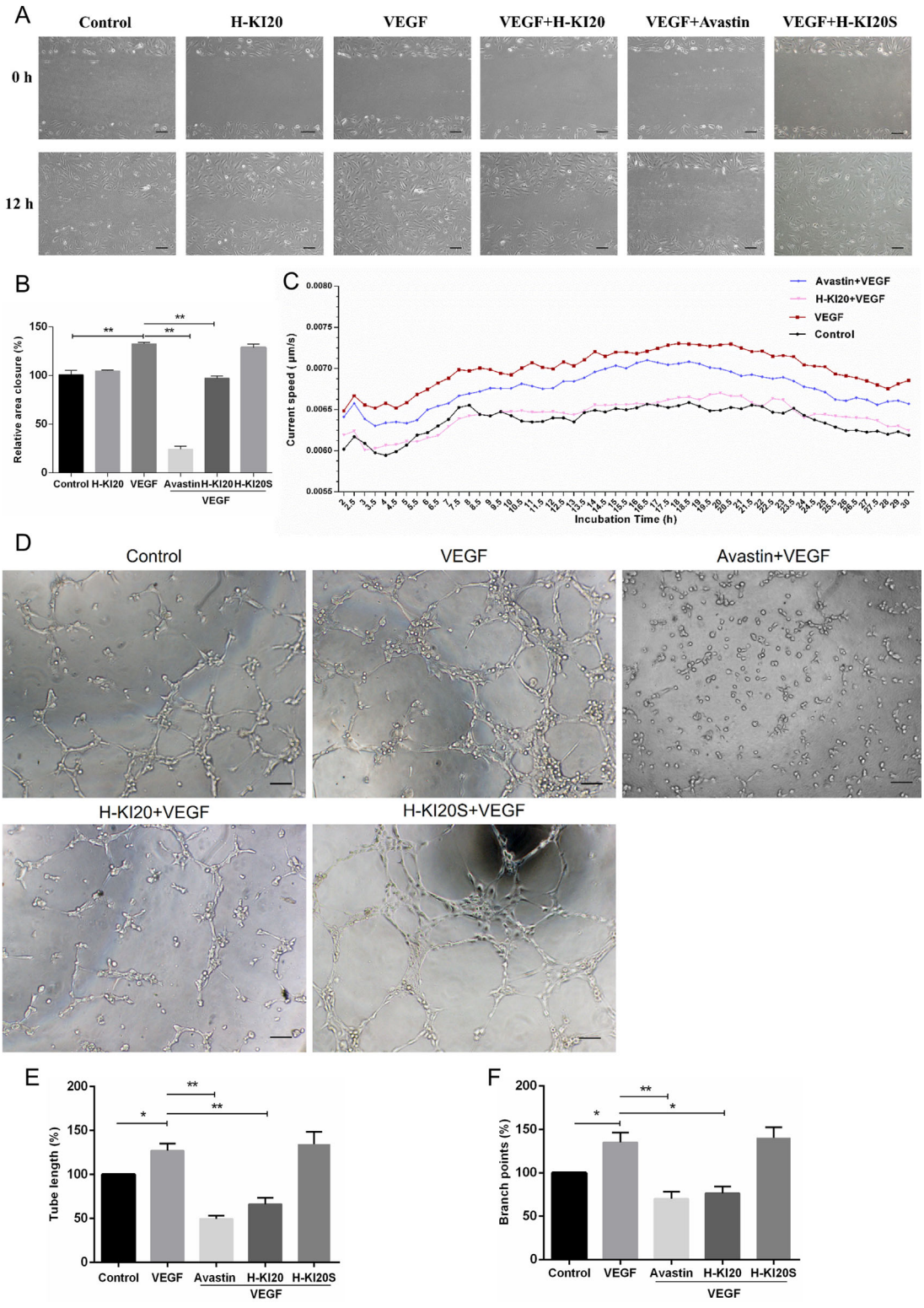

Figure 2. H-KI20 inhibited angiogenesis of HRECs induced by VEGF. (**A** and **B**) The inhibitory effects of H-KI20 on the migration of HRECs stimulated by VEGF. (**A**) Representative images of HRECs' migration after incubation with VEGF, Avastin, H-KI20 and H-KI20S (scramble peptide) at 0 and 12 h. *Scale bar*: 50 μm. (**B**) Quantitative analysis of HRECs migration, the relative area closure of three random fields was calculated for each group, and normalized to the Control group. Three independent assays were performed, and data are shown as means ± SEM, $^{*}P < 0.05$, $^{**}P < 0.01$. (**C**) The current movement speed of HRECs incubated with VEGF, Avastin and H-KI20 from two to 30 hours was analyzed by Operetta HCA system (PerkinElmer), with an interval of 0.5 hour. (**D**) Representative images of HRECs' tube formation after incubation with VEGF, Avastin, H-KI20 and H-KI20S (scramble peptide) for three hours. *Scale bar*: 50 μm. (**E** and **F**) Quantification of total tube length and branch points related to (**D**). Three independent assays were performed, and data are presented as mean ± SEM, $^{*}P < 0.05$, $^{**}P < 0.01$.

Investigative Ophthalmology & Visual Science

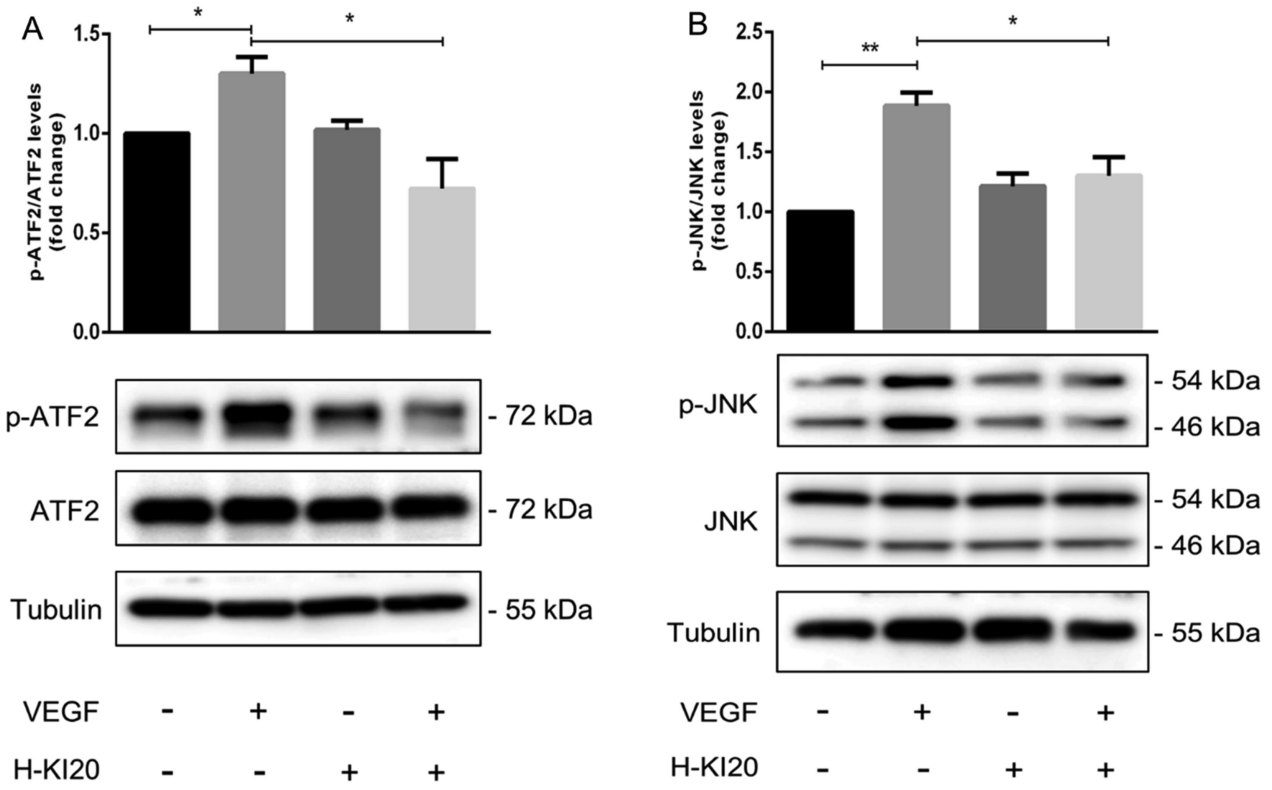

Figure 3. H-KI20 inhibited VEGF-stimulated phosphorylation of ATF2 and JNK. HRECs were pretreated with H-KI20 for 24 hours before stimulation with or without VEGF for 15 minutes. Protein expression of ATF2 and p-ATF2 (**A**) and JNK and p-JNK (**B**) were analyzed by Western blotting. Densitometric analysis of Western blot images of p-ATF2 over ATF2 and p-JNK over JNK was performed. Three independent experiments were performed, and data were expressed as means± SEM when compared to untreated cells, $^{*}P < 0.05$, $^{**}P < 0.01$.

residues Gln[28], Ala[53], Arg[69], Glu[73], Ile[148], Asp[151], and Asp[169] in JNK2 were involved in binding with Lys[20], Thr[15], Ile[1], Ile[14], Lys[9], Ser[7], and Ser[13], respectively, in H-KI20 through hydrogen bond interactions. In addition, the oxygen atom of the carboxyl group of Asp[169] in JNK2 formed a salt bridge with the nitrogen atom of the guanidine group of Arg[6] in H-KI20. Finally, the change in response unit after JNK2 incubation with a range of concentrations of H-KI20 was monitored to directly test and quantify the interaction between H-KI20 and JNK2. As shown in Figure 5C, the binding isotherms showed the direct binding of H-KI20 to JNK2, with dissociation constant (K_d) values of 83.68 µM.

H-KI20 Inhibited Angiogenesis in Vivo by Using the CAM and OIR Model

The CAM and OIR models were used to explore whether H-KI20 suppressed angiogenesis in vivo. The number of vessels in the black ring decreased by 46.3% in the H-KI20 group compared to that in the PBS group (Figs. 6A and 6B), whereas H-KI20S (scrambled peptide) did not exert any antiangiogenic effects. In the OIR model, the number of retinal vascular tufts decreased by 63.6% or 72.1% in the H-KI20 or VEGFab (VEGF antibody) group, respectively, compared to oxygen + PBS group; however, no significant difference was found between the oxygen + H-KI20S and oxygen + PBS groups (Figs. 6C and 6D). Meanwhile, the number of vascular tufts in HE-stained retinal sections increased in the oxygen + PBS and oxygen + H-KI20S groups compared to the room air +PBS group, and these abnormalities were significantly alleviated by H-KI20 and VEGFab (Fig. 6E).

Discussion

Multiple studies reported that peptides targeted extracellular matrix proteins, cell surface receptors, and growth factors to suppress angiogenesis. For example, Angio-3, a peptide derived from plasminogen kringle 3, inhibited angiogenesis and vascular permeability by suppressing the dissociation of ZO-1 and ZO-2 from tight junctions and VE-cadherin from adherent junctions induced by VEGF.[42] Another peptide, AXT107, derived from tyrosine kinase blocking collagen IV, inhibited subretinal neovascularization through binding to $\alpha v\beta 3$ integrins, reducing the phosphorylation of vascular endothelial growth factor receptor 2 (VEGFR2) and increasing the internalization, ubiquitination and degradation of VEGFR2.[43]

Our previous study showed that peptide H-KI20 inhibited VEGF and intrastromal suture–induced cornea neovascularization *in vivo*, and the topical application of high concentrations of H-KI20 exerted no effect on the cell ultrastructure of cornea and conjunctiva.[44] This study further illustrated that H-KI20 had an excellent capability in inhibiting the key biological characteristics in angiogenesis, including the migration, tube formation, and movement speed of HRECs induced by VEGF without affecting cell morphology in vitro (Figs. 1 and 2). In addition, the proliferation of HRECs was not suppressed by H-KI20, and all layers of the retina were normal and intact on five days after

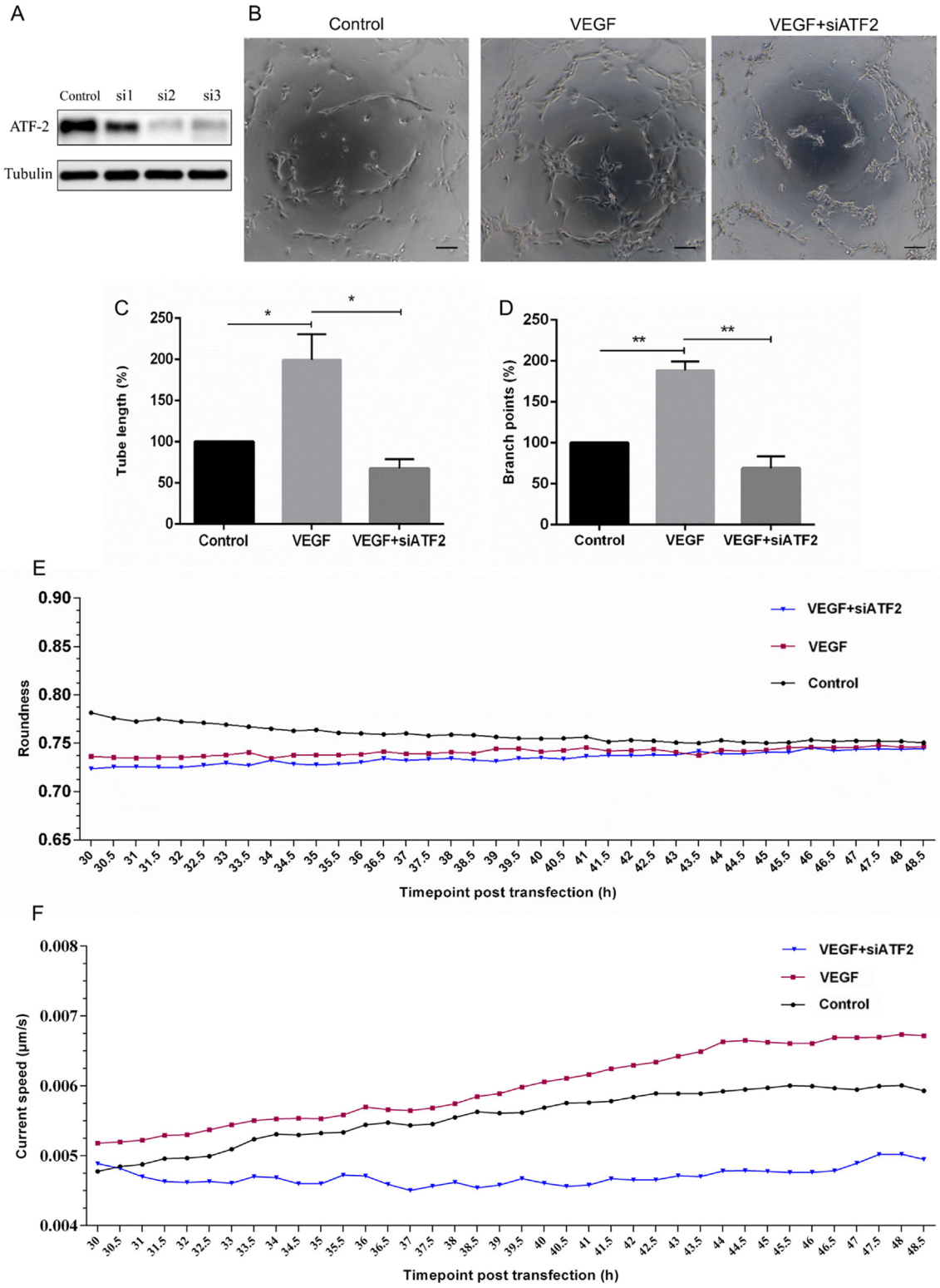

Figure 4. The knockdown of ATF2 attenuated HRECs' tube formation and movement speed. (**A**) Western blot analysis of ATF2 in HRECs transfected with ATF2 siRNA or the control vector. Three different siRNAs were evaluated for the efficiency of ATF2 expression inhibition, ATF2-siRNA1 (si1), ATF2-siRNA2 (si2), and ATF2-siRNA3 (si3). (**B**) Representative images of HRECs' tube formation at 48 hours after transfection with ATF2 si2 or the control vector. *Scale bar*: 50 μm. (**C** and **D**) Quantification of total tube length and branch points related to (**B**). Three independent experiments were performed, and data are presented as means ± SEM, $^{*}P < 0.05$, $^{**}P < 0.01$. (**E**) Cell roundness and (**F**) current movement speed were analyzed by Operetta HCA system (PerkinElmer) from 30 hours to 48.5 hours after ATF2 si2 transfection, with an interval of 0.5 hour.

Investigative Ophthalmology & Visual Science

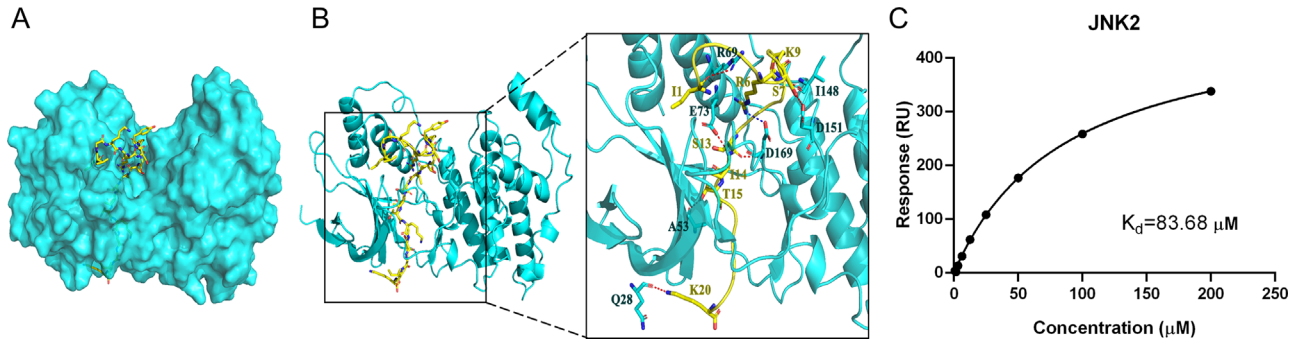

Figure 5. H-KI20 bound JNK2 directly. (**A** and **B**) Binding pose and interactions of H-KI20 with JNK2. (**A**) The surface binding model of H-KI20 with JNK2. (**B**) The detailed interaction between H-KI20 and JNK2. The residues in JNK2 are colored in *cyan* and residues in H-KI20 are colored in *yellow*. The *red dashes* represent hydrogen bond interaction, and the *blue dashes* indicate the salt bridge. (**C**) Increased response unit after the incubation of JNK2 with a various concentrations of H-KI20. The K_d value was determined by global fitting to a Langmuir 1:1 binding model within the Biacore Evaluation software (GE Healthcare).

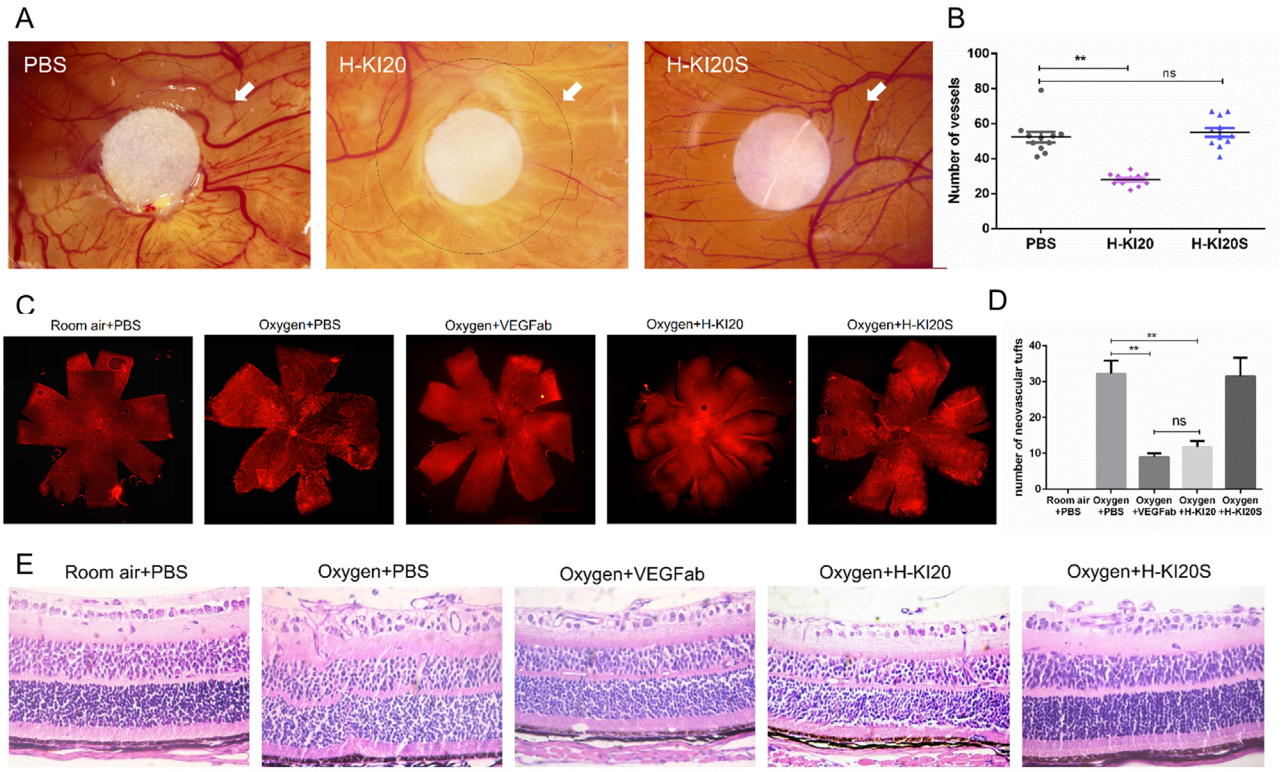

Figure 6. H-KI20 inhibited angiogenesis in CAM and OIR models. (**A**) Representative images of CAM treated with PBS, H-KI20 and H-KI20S (scramble peptide) for 72 hours. Magnification ×11.5. (**B**) Quantification of vessels surrounding the filter disk within the black ring (*white arrow*, **A**) indicated 2.5 mm around the filter paper. Data are presented as means ± SEM, $^{**}P < 0.01$, $n = 11$ per group. In OIR model (**C, D,** and **E**), (**C**) isolectin B4 (IB4) staining of retina at P17 from mice exposed to room air or 75% ± 2% oxygen with intravitreal injections of PBS, VEGFab,H-KI20, or H-KI20S (scramble peptide). Magnification ×40. (**D**) Quantification of vascular tufts related to (**C**). Data are presented as mean ± SEM, $^{**}P < 0.01$, $n = 4$ per group. (**E**) Vascular lumens (vascular tufts extending from the retinal surface to vitreous cavity) were shown in sections stained with HE. Magnification ×400. $n = 6$ per group.

intravitreal injection, without edema or immune reactions (Supplementary Figs. S2C and S2D), supporting the low immunogenicity of H-KI20. Compared to 2.5 mg/mL Avastin, a lower concentration of H-KI20 (200 μM, 0.4 mg/mL) inhibited cell motility. The current speed of HRECs decreased from 8.5 hours till the end of the assay by HCA (Fig. 2C). And H-KI20 reversed the migration of VEGF-stimulated cells back to the level of the control group, which was not as effective as 12.5 mg/mL Avastin treatment (Fig. 2A and Supplementary Fig. S4), implying that H-KI20 inhibited migration induced by VEGF without collateral damage to normal cellular function. In addition, several studies reported that a reduced response to Avastin and Lucentis in nAMD over a longer period of use, associated with downregulation of antiangiogenic factors or upregulation of proangiogenic factors other than VEGF-A, including VEGF-B and

Investigative Ophthalmology & Visual Science

Table. The Docking Scores of Peptide H-KI20 With 29 Upstream Proteins Regulating ATF2 Proteins, Including JNK2

Receptor	Docking Score (kcal/mol)*
JNK2	−18.97
JNK3	−18.28
ERK1	−17.71
MAPK14	−17.41
MKK7	−17.34
MAPK11	−16.42
RAF	−16.27
MKK4	−16.22
CRKL	−15.68
JNK1	−15.68
MEK2	−15.65
PAK1	−15.38
PAK4	−15.34
GCK	−15.24
SRC	−15.22
ERK2	−15.09
PAK3	−14.50
Hpk1	−14.19
MKK6	−13.98
Sos1	−13.92
RAL	−13.07
RAC1	−12.75
Shc1	−12.56
CDC42	−12.23
Sos2	−12.19
MLK3	−12.04
ASK1	−11.92
Tak1	−11.39
MLK2	−10.48

* Docking score were calculated by the GBVI/WSA ΔG, which is a forcefield-based scoring function, estimating the free energy of binding of the ligand from a given pose. A more negative score indicates a better binding of peptide with protein.

placental growth factor (PlGF).[45] Both VEGF-B and PlGF could activate the JNK signaling pathway.[46,47] Our finding that H-KI20 boosted the efficacy of Avastin inhibiting the migration of HRECs (Supplementary Fig. S5), together indicated the potential of H-KI20 in decreasing the dose or frequency of Avastin. Meanwhile, the retinal pathological neovascularization was inhibited by H-KI20 whereas the retinal vasculature remained normal in the OIR mouse model (Fig. 6), supporting the in vivo efficiency of H-KI20.

The present study further characterized the cellular mechanisms of H-KI20 peptide, which reduced phosphorylation of ATF2 induced by VEGF (Fig. 3). The increased expression and phosphorylation of ATF2 showed an association with increased tumor aggressiveness in patients with Paget's disease, indicating the involvement of ATF2 in cellular invasion and migration.[23] In addition, few studies reported the contribution of ATF2 in ocular diseases. In one study, ATF2 acted as a downstream mediator of death of the RGCs, possibly causing axon degeneration after axonal injury.[27] In another study, the expression level of ATF-2 increased in the retina of Akita mice, which is a type 1 diabetic model. The results showed that increased ATF2 expression promoted the proliferation, migration, and metabolism of RPE cells in DR.[28] In the present study, ATF2 knockdown through siRNA transfection reduced tube formation and movement speed of HRECs (Fig. 4), indicating the pivotal role of ATF2 in VEGF-induced retinal neovascularization. The phosphorylation of ATF2 on Thr 69 and Thr 71 was mediated by JNK or p38.[48,49,50] Besides, certain growth factors such as insulin and EGF activated ATF2 that are phosphorylated through ERK-independent phosphorylation on Thr71, followed by p38-dependent phosphorylation on Thr69.[51] This study revealed that VEGF increased the phosphorylation of ATF2 on Thr 69 and Thr 71 through JNK, but not through p38 in HRECs. This discrepancy might be associated with the use of different cell lines in various studies. HRECs are primary human retinal microvascular endothelial cells that better mimics the real situation in humans. The docking results (Table) indicated that H-KI20 had a high-affinity binding to JNK2 with binding energy of −18.97 kcal/mol. The docking simulation studies also implied that H-KI20 bound to JNK2 through salt bridges and seven hydrogen bond interactions. In addition, the binding affinity of JNK2 with H-KI20 was determined using SPR, with dissociation constant (K_d) values of 83.68 µM (Fig. 5), indicating that H-KI20 could inhibit angiogenesis through targeting JNK2. However, this K_d value suggested a relatively low binding affinity, indicating other possible mechanisms of action, including other candidates listed in Table, which can be further investigated in the future.

Last but not least, the short half-life of peptides is a major limitation intreating ocular diseases due to potential degradation by proteases.[14,52] The concentration of H-KI20 was stable in a variety of aqueous solutions for a minimum of 48 hours, especially in BSS Plus, which is used in all intraocular surgical procedures supplemented with glutathione, dextrose and sodium bicarbonate based on conventional BSS, mimicking aqueous and vitreous humors.[53] Chemical modifications might be adopted, including cyclization, substituting D-amino acids for L-amino acids, end modification, conjugation with polyethylene glycol (PEG) and commination of various modifications to further increase the half-life of H-KI20 in vivo.[14] H-KI20 was stable in BSS PLUS (Supplementary Fig. S2), and FITC-labeled H-KI20 displayed excellent penetration ability in vitro and in vivo (CNV model) (Fig. 1). Moreover, concentrations of H-KI20 in different ocular tissues at different times after topical instillation were measured using PRM assay, which also illustrated the excellent penetration ability of H-KI20 in vivo. We speculated that H-KI20 might has the potential as eye drops during intravitreal injections of Avastin to consolidate efficacy and decrease the frequency of Avastin. Taken together, H-KI20 acted as a potential drug precursor for treating ocular neovascular diseases and is worthy of further investigation in the future.

Acknowledgments

The authors thank Shengru Pang's assistance on high-content analysis system, Jing Hu for technical assistance with the CNV assay, and Chenhao Pan for technical guidance.

Supported by grants from the National Natural Science Foundation of China (No. 81700844, No. 81970810, No. 81800835), National Key R&D Program of China (2016YFC0904800, 2019YFC0840607) and National Science and Technology Major Project of China (2017ZX09304010), Shanghai Sailing Program (18YF1419700), Shanghai "Rising Stars of Medical Talent" Youth Development Program, Basic research and cultivation project of Shanghai Eye Disease Prevention and Treatment Center (20JC01001).

Disclosure: **R. Wang,** None; **Y. Xu,** None; **C. Niu,** None; **X. Gao,** None; **X. Xu,** None

References

1. Sabanayagam C, Banu R, Chee ML, et al. Incidence and progression of diabetic retinopathy: a systematic review. *Lancet Diabetes Endocrinol.* 2019;7:140–149.
2. Lim LS, Mitchell P, Seddon JM, et al. Age-related macular degeneration. *Lancet.* 2012;379:1728–1738.
3. Hellström A, Smith LE, Dammann O. Retinopathy of prematurity. *Lancet.* 2013;382:1445–1457.
4. Hu J, Dziumbla S, Lin J, et al. Inhibition of soluble epoxide hydrolase prevents diabetic retinopathy. *Nature.* 2017;552:248–252.
5. Risau W. Mechanisms of angiogenesis. *Nature.* 1997;386:671–674.
6. Carmeliet P, Jain RK. Molecular mechanisms and clinical applications of angiogenesis. *Nature.* 2011;473:298–307.
7. Watanabe D, Suzuma K, Matsui S, et al. Erythropoietin as a retinal angiogenic factor in proliferative diabetic retinopathy. *N Engl J Med.* 2005;353:782–792.
8. Gross JG, Glassman AR, Jampol LM, et al. Panretinal photocoagulation vs intravitreous ranibizumab for proliferative diabetic retinopathy: a randomized clinical trial. *JAMA.* 2015;314:2137–2146.
9. Wells JA, Glassman AR, Ayala AR, et al. Aflibercept, bevacizumab, or ranibizumab for diabetic macular edema. *N Engl J Med.* 2015;372:1193–1203.
10. Chakravarthy U, Harding SP, Rogers CA, et al. Alternative treatments to inhibit VEGF in age-related choroidal neovascularisation: 2-year findings of the IVAN randomised controlled trial. *Lancet.* 2013;382:1258–1267.
11. Sadda SR, Tuomi LL, Ding B, et al. Macular atrophy in the HARBOR study for neovascular age-related macular degeneration. *Ophthalmology.* 2018;125:878–886.
12. Bracha P, Moore NA, Ciulla TA, et al. The acute and chronic effects of intravitreal anti-vascular endothelial growth factor injections on intraocular pressure: a review. *Surv Ophthalmol.* 2018;63:281–295.
13. Zhao H, Jin H, Li Q, et al. Inhibition of pathologic retinal neovascularization by a small peptide derived from human apolipoprotein(a). *Invest Ophthalmol Vis Sci.* 2009;50:5384–5395.
14. Sulochana KN, Ge R. Developing antiangiogenic peptide drugs for angiogenesis-related diseases. *Curr Pharm Des.* 2007;13:2074–2086.
15. Sima J, Zhang SX, Shao C, et al. The effect of angiostatin on vascular leakage and VEGF expression in rat retina. *FEBS Lett.* 2004;564:19–23.
16. Kunio M, Toshikazu N. Mechanisms and significance of bifunctional NK4 in cancer treatment. *Biochem Biophys Res Commun*. 2005;333:316–27.
17. Al-Horani Rami A, Desai Umesh R. Recent advances on plasmin inhibitors for the treatment of fibrinolysis-related disorders. *Med Res Rev*. 2014;34:1168–216.
18. Xin L, Xu R, Zhang Q, et al. Kringle 1 of human hepatocyte growth factor inhibits bovine aortic endothelial cell proliferation stimulated by basic fibroblast growth factor and causes cell apoptosis. *Biochem Biophys Res Commun.* 2000;277:186–190.
19. Shen Z, Yang ZF, Gao Y, et al. The kringle 1 domain of hepatocyte growth factor has antiangiogenic and antitumor cell effects on hepatocellular carcinoma. *Cancer Res.* 2008;68:404–414.
20. Estrada Chelsea C, Maldonado A, Mallipattu Sandeep K. Therapeutic Inhibition of VEGF Signaling and Associated Nephrotoxicities. *J Am Soc Nephrol.* 2019;30:187–200.
21. Tate Courtney M, Wayne B, Lisa W, et al. LY2228820 dimesylate, a selective inhibitor of p38 mitogen-activated protein kinase, reduces angiogenic endothelial cord formation in vitro and in vivo. *J Biol Chem.* 2013;288:6743–53.
22. Zhuo H, Zhao Y, Cheng X, et al. Tumor endothelial cell-derived cadherin-2 promotes angiogenesis and has prognostic significance for lung adenocarcinoma. *Molecular Cancer.* 2019;18(1):34.
23. Lopez-Bergami P, Lau E, Ronai Z. Emerging roles of ATF2 and the dynamic AP1 network in cancer. *Nat Rev Cancer.* 2010;10:65–76.
24. Bhoumik A, Takahashi S, Breitweiser W, et al. ATM-dependent phosphorylation of ATF2 is required for the DNA damage response. *Mol Cell.* 2005;18:577–587.
25. Endo M, Su L, Nielsen TO. Activating transcription factor 2 in mesenchymal tumors. *Hum Pathol.* 2014;45:276–284.
26. Maekawa T, Jin W, Ishii S. The role of ATF-2 family transcription factors in adipocyte differentiation: antiobesity effects of p38 inhibitors. *Mol Cell Biol.* 2010;30:613–625.
27. Welsbie DS, Mitchell KL, Jaskula-Ranga V, et al. enhanced functional genomic screening identifies novel mediators of dual leucine zipper kinase-dependent injury signaling in neurons. *Neuron.* 2017;94:1142–1154.
28. Shao Y, Dong LJ, Takahashi Y, et al. miRNA-451a regulates RPE function through promoting mitochondrial function in proliferative diabetic retinopathy. *Am J Physiol Endocrinol Metab.* 2019;316:E443–E452.
29. Xu Y, Zhao H, Zheng Y, et al. A novel antiangiogenic peptide derived from hepatocyte growth factor inhibits neovascularization in vitro and in vivo. *Mol Vis.* 2010;16:1982–1995.
30. Chen C, Liu K, Xu Y, et al. Anti-angiogenesis through noninvasive to minimally invasive intraocular delivery of the peptide CC12 identified by in vivo-directed evolution. *Biomaterials.* 2017;112:218–233.
31. Liu C, Tai L, Zhang W, et al. Penetratin, a potentially powerful absorption enhancer for noninvasive intraocular drug delivery. *Mol Pharm.* 2014;11:1218–1227.
32. Ma J, Wang Q, Fei T, et al. MCP-1 mediates TGF-beta-induced angiogenesis by stimulating vascular smooth muscle cell migration. *Blood.* 2007;109:987–994.
33. Li J, Cubbon RM, Wilson LA, et al. Orai1 and CRAC channel dependence of VEGF-activated Ca2+ entry and endothelial tube formation. *Circ Res.* 2011;108:1190–1198.
34. Geng J, Wang Y, Zhang L, et al. The cajanine derivative LJ101019C regulates the proliferation and enhances the activity of NK cells via Kv1.3 channel-driven activation of the AKT/mTOR pathway. *Phytomedicine.* 2020;66:153113.
35. Lambert V, Lecomte J, Hansen S, et al. Laser-induced choroidal neovascularization model to study age-related macular degeneration in mice. *Nature Protocols*, 2013;8(11):2197–2211.
36. Kim KH, Lee SY, Kim DG, Lee SY, Kim JY, Yoo JS. Absolute quantification of *N*-glycosylation of alpha-fetoprotein using parallel reaction monitoring with stable isotope-labeled-glycopeptide as an internal standard. *Anal Chem*. 2020;92:12588–12595.
37. Danese S, Sans M, Motte de la C, et al. Angiogenesis as a novel component of inflammatory bowel disease pathogenesis. *Gastroenterology.* 2006;130:2060–2073.
38. Connor KM, Krah NM, Dennison RJ, et al. Quantification of oxygen-induced retinopathy in the mouse: a model of vessel loss, vessel regrowth and pathological angiogenesis. *Nat Protoc.* 2009;4:1565–1573.
39. Ruddarraju RR, Murugulla AC, Kotla R, et al. Design, synthesis, anticancer, antimicrobial activities and molecular docking studies of theophylline containing acetylenes and theophylline containing 1,2,3-triazoles with variant nucleoside derivatives. *Eur J Med Chem*. 2016, 123:379–396.
40. Mohammadzadeh-Asl S, Aghanejad A, Yekta R, et al. Kinetic and thermodynamic insights into interaction of erlotinib

with epidermal growth factor receptor: surface plasmon resonance and molecular docking approaches. *Int J Biol Macromol.* 2020;163:954–958.

41. Georgalas I, Koutsandrea C. Approve bevacizumab for use in eye disease in cash strapped times. *BMJ.* 2012;345:e4806.
42. Venugopal S, Kao C, Chandna R, et al. Angio-3, a 10-residue peptide derived from human plasminogen kringle 3, suppresses tumor growth in mice via impeding both angiogenesis and vascular permeability. *Angiogenesis.* 2018;21:653–665.
43. Silva RLE, Kanan Y, Mirando AC, et al. Tyrosine kinase blocking collagen IV-derived peptide suppresses ocular neovascularization and vascular leakage. *Sci Transl Med.* 2017;9:eaai8030.
44. Lu Y, Xu Y, Gu Q, et al. Inhibition of pathologic corneal neovascularization by topical application of a novel peptide in vivo. *Cornea.* 2015;34:1295–1302.
45. Stefano L, Guido R, Sole SM, et al. Aflibercept administration in neovascular age-related macular degeneration refractory to previous anti-vascular endothelial growth factor drugs: a critical review and new possible approaches to move forward. *Angiogenesis.* 2015;18(4):397–432.
46. Gonsalves Caryn S, Scott C, Sharat C, et al. Angiogenic growth factors augment K-Cl cotransporter expression in erythroid cells via hypoxia-inducible factor-1α. *Am J Hematol.* 2014;89:273–281.
47. Wang P, Chen S-H, Hung W-C, et al. Fluid shear promotes chondrosarcoma cell invasion by activating matrix metalloproteinase 12 via IGF-2 and VEGF signaling pathways. *Oncogene.* 2015;34:4558–4569.
48. Gu L, Larson Casey JL, Andrabi SA, et al. Mitochondrial calcium uniporter regulates PGC-1alpha expression to mediate metabolic reprogramming in pulmonary fibrosis. *Redox Biol.* 2019;26:101307.
49. Cuhlmann S, Van der Heiden K, Saliba D, et al. Disturbed blood flow induces RelA expression via c-Jun N-terminal kinase 1: a novel mode of NF-kappaB regulation that promotes arterial inflammation. *Circ Res.* 2011;108:950–959.
50. Gupta S, Campbell D, Derijard B, et al. Transcription factor ATF2 regulation by the JNK signal transduction pathway. *Science.* 1995;267:389–393.
51. Ouwens DM, de Ruiter ND, van der Zon GC, et al. Growth factors can activate ATF2 via a two-step mechanism: phosphorylation of Thr71 through the Ras-MEK-ERK pathway and of Thr69 through RalGDS-Src-p38. *EMBO J.* 2002;21:3782–3793.
52. Yun JA, Kim J, Baek YY, et al. N-terminal modification of the tetrapeptide Arg-Leu-Tyr-Glu, a vascular endothelial growth factor receptor-2 (VEGFR-2) antagonist, improves antitumor activity by increasing its stability against serum peptidases. *Mol Pharmacol.* 2019;96:692–701.
53. Edelhauser HF, Gonnering R, Van Horn DL. Intraocular irrigating solutions. A comparative study of BSS Plus and lactated Ringer's solution. *Arch Ophthalmol.* 1978;96:516–520.

Investigative Ophthalmology & Visual Science